Vibrational properties and infrared spectra of $Al_xGa_{1-x}As$ systems. I. Average-t-matrix approximation versus supercell calculation for homogeneous alloys

M. Bernasconi and L. Colombo*
Scuola Internazionale Superiore di Studi Avanzati (SISSA), Strada Costiera 11, I-34014 Grignano, Trieste, Italy

L. Miglio and G. Benedek
Dipartimento di Fisica dell'Università di Milano, via Celoria 16, I-20133 Milano, Italy
(Received 8 October 1990; revised manuscript received 26 December 1990)

We calculate the optical properties of the $Al_xGa_{1-x}As$ mixed crystal in a bond-charge-model, average-t-matrix-approximation (ATA), and mass-defect scheme. Comparison is made with numerical results obtained by a supercell procedure and with recent experimental measurements. The predictive power and the limits of the perturbative approach in the 50% concentration range are discussed, in view of a useful application of the ATA technique to the $Al_xGa_{1-x}As$ superlattices, which will be investigated in the following paper.

I. INTRODUCTION

The recent development of epitaxial-growth techniques has renewed a strong interest in the spectral properties of mixed III-V compounds. In fact, it is now possible to tune exactly the Al content x in $Al_xGa_{1-x}As$ mixtures, to alternate different concentrations in $Al_xGa_{1-x}As/Al_yGa_{1-y}As$ superlattices, or even to modulate the composition x as a smooth periodic function along the growth axis, as is the case of modulated alloys. In the latter situations, an interesting problem arises, i.e., which are the dynamical effects of *macroscopic order* (such as superperiodicity) when superimposed on the microscopic disorder of a mixed crystal. This problem will be investigated in the companion paper of ours[1] (hereafter referred to as II); still we need a reliable tool for the calculation of the vibrational spectra of compositionally disordered materials. The virtual crystal approximation (VCA) is not suitable for two-mode-behaved systems,[2] however it can be used as a starting point for single-site-scattering perturbative techniques, such as the average-t-matrix approximation (ATA) and coherent potential approximation (CPA).[3] The latter is a powerful self-consistent approach recently used for III-V compounds in the framework of simplified dynamical models.[4,5] As a matter of fact, the application to superlattices and modulated alloys in the framework of a three-dimensional, sophisticated dynamics (such as the bond-charge-model, BCM) requires a less computer-time technique, i.e., the ATA.

In the present paper we investigate the predictive power and the limits of a BCM-ATA approach for the calculation of some optical properties of the $Al_xGa_{1-x}As$ system, such as Im $\tilde{\chi}(\omega)$, $-\mathrm{Im}\tilde{\epsilon}^{-1}(\omega)$, and reflectivity response functions. The critical region where the ATA interpolation scheme is known to be poor, is the 50% concentration range: Here an extensive comparison is made to supercell calculations (up to 960 atoms), in the framework of the BCM dynamics.

Very recent Raman measurements on $Al_xGa_{1-x}As$ samples, grown by molecular-beam epitaxy,[6] display several minor features, which are still a matter of discussion in current literature. Comparison to $-\mathrm{Im}\tilde{\epsilon}^{-1}(\omega)$ calculated by the ATA and supercell (SC) approaches may be helpful in order to understand if they represent either extrinsic or intrinsic effects. However, a quantitative analysis requires the calculation of the Raman intensities, a task which is presently in progress and will be the subject of a forthcoming publication by us.

In Sec. II we review the state of the art for the optical properties of $Al_xGa_{1-x}As$ systems and point out the relevant features which are expected to be reproduced by a reliable calculation. Section III provides a survey of the BCM scheme, its advantages and drawbacks, and a discussion of the mass-defect (MD) approximation, here adopted for AlAs dynamics. The ATA and SC techniques are outlined in Secs. IV and V, respectively, whereas in Sec. VI we explain how the dielectric properties of the mixed crystal have been calculated. The results of both ATA and SC calculations along with the final conclusions of the present work are contained in Sec. VII.

II. OPTICAL PROPERTIES OF $Al_xGa_{1-x}As$

A fair amount of Raman data has been collected for $Al_xGa_{1-x}As$, especially in relation to the interpretation of disorder-activated structures in the low-energy part of the spectrum (for a review see Ref. 7, and references quoted therein). In regard to infrared absorption (ir) and reflectivity measurements, only a couple of systematic investigations are present in literature by Ilegemes and Pearson (1970) and by Kim and Spitzer (1979).[8] The two reflectivity measurements substantially agree in finding no significant ir-active modes in $Al_xGa_{1-x}As$ other than two dominant reststrahlen bands close to the optical modes of pure GaAs and pure AlAs, respectively. The two-mode behavior is typical of mixed crystals for which

the optical bands of pure materials do not overlap and where, near the extremes of the composition range, the localized mode of the minority ions lies well outside the reststrahlen peak of the host crystal. By Kramer-Kronig transformation the shift in frequency with Al concentration for the GaAs-like and AlAs-like LO and TO peaks has been carefully studied by Kim and Spitzer.[8] The reflectivity spectra of Ilegemes and Pearson, however, do cover a wide range for x and our calculations will also be compared to them. A two-mode behavior is observed for Raman peaks associated to LO phonons[9] as well. Moreover, disorder-activated-transverse-acoustic (DATA) and longitudinal-acoustic (DALA) bands are evidenced in resonant conditions, as caused by the relaxation of the crystal momentum conservation rule due, in turn, to the lack of lattice periodicity: disorder-activated optical (DAO) modes are also present just beneath GaAs-like and AlAs-like LO peaks.[9] The absence of other structures in the Raman spectra for the optical vibrations and in the reflectivity curves may suggest that the impurity distribution in the metallic sublattice is essentially homogeneous, i.e., no cluster modes are resolved in the experimental measurements. Consequently, the perturbative approach to configurationally averaged Green functions[3] can provide realistic spectra, especially in our case, where a supercell calculation is also performed. Actually, some theoretical models for the lattice dynamics of $Al_xGa_{1-x}As$ have been alternatively proposed as complementary investigation: Kobayashi, Dow, and O'Reilly[10] performed a numerical calculation on a 1000-atom cluster, by means of the recursion method technique; Bonneville[5] treated the mass defect in the CPA scheme and the off-diagonal disorder just at the VCA step, since the modifications in the force constants are well known to be of minor importance in this system. However, both these calculations of the phonon spectra employed Born-Von Karman dynamics or crudely simplified shell models (no Coulombic interactions, for instance) and, moreover, no disorder in the effective charges is comprised.

The Raman spectra in the limits $x \sim 0,1$ have been investigated by Talwar, Vandevyver, and Zigone,[1] in the framework of a 11-parameter rigid-ion model for the isolated defect. Here, in our opinion, the role of force-constant changes with composition is overestimated. In fact, vibrational properties of homogeneous alloys have been studied very recently by means of *ab initio* linear-response density-functional theory by Baroni *et al.*[12] Both dispersion relations and the Raman spectrum for the 50% Al concentration alloy have been calculated showing that the force-constant changes between AlAs and GaAs are negligible. Despite the advances in *ab initio* calculations, the phenomenological model used in the present calculations (see the following section) still preserves some advantages: (i) it displays a large flexibility in dealing with extended calculations, especially for the case of superlattices and modulated alloys; (ii) no realistic phonon densities of states for the homogeneous alloys (such as the ones here reported) are, to our knowledge, presently available.

III. DYNAMICAL MODEL

Both for ATA and SC calculations we adopted the adiabatic BCM, originally developed by Weber for bulk dispersion relations in homopolar semiconductors[13] and III-V compounds.[14] This model is characterized by the presence of bond charges (BC) placed along the tetrahedral covalent bonds as predicted by *ab initio* calculations and experimental measurements.[15] A suitable modeling of the electronic degrees of freedom allows, in turn, a good description of the dispersion relations with a limited set of parameters. In fact, only six of them are included in the BCM for III-V compounds, namely, cation-anion, cation-BC, and anion-BC short-range central interactions; BC-BC angular potential (Keating-like) around each ion and Coulomb interactions between all the charged particles of the crystal. The latters are generated by a standard Ewald summation[16] with one parameter only, i.e., the BCM effective charge $Z^*/\sqrt{\epsilon}$. In contrast to other microscopic models (such as the shell model) even with a large set of parameters, the BCM does provide the correct zone-boundary flattening of the TA branches, one particularly important feature for the analysis of DATA structures with respect to resonant Raman measurements.[9] Recently, the microscopic soundness of the BCM has been proved by comparison between BCM and *ab initio* interplanar force constants[17,18] and by neutron-scattering measurements by Strauch and Dorner.[19]

We evaluated the GaAs bulk dynamics by the set of parameters contained in Ref. 14. In regards to AlAs, few experimental data (only at zone center and questionable at zone boundary) are presently available,[20] consequently the fitting procedure of the BCM parameters is somewhat arbitrary. In order to bypass any arbitrariness in the fitting procedure, the present calculation is performed within the MD approximation suggested by *ab initio* results by Baroni *et al.*,[12] which, moreover, turns out to be a necessary condition for SC and ATA approaches to mixed $Al_xGa_{1-x}As$ systems. Our results for bulk AlAs are in good agreement with the few experimental data,[20] except for a too large dispersion of the optical branches at the M point of the Brillouin zone, which promptly disappears as soon as a few Ga impurities are present: Just our case.

One final comment still deserves the evaluation of the transverse effective charge Z, needed for the calculation of the dielectric susceptibility (see Sec. VI): The value of Z can be consistently derived from the parameters of the present model. One possible way to derive it is to identify the denominator $\sqrt{\epsilon}$ of the BCM parameter $Z^*/\sqrt{\epsilon}$ as the dielectric screening provided by the multipolar deformation of the valence charge, not described by the point-like nature of the bond charges. Following this approach in the simultaneous evaluation of the transverse effective charge Z and electronic static dielectric constant ϵ_∞, one obtains $\epsilon = 4.488$ and $Z = 2.165$. Probably, this excellent agreement to the value obtained from the LO-TO splitting and the experimental value of ϵ_∞, is partially accidental, by considering the lack of interatomic charge

transfer during the ionic motion[21] in the BCM, but it confirms that the electronic response is correctly described by the model.

IV. AVERAGE t-MATRIX-APPROXIMATION FOR MIXED CRYSTALS

In order to correctly reproduce the dynamical features of a disordered crystal, it is necessary to evaluate configuration averages: To this aim we must calculate the configuration-averaged perturbed Green function $\langle \overleftrightarrow{G} \rangle$ by means of a translational invariant Dyson equation[3]

$$\langle \overleftrightarrow{G} \rangle = \overleftrightarrow{G}_0 + \overleftrightarrow{G}_0 \overleftrightarrow{\Sigma} \langle \overleftrightarrow{G} \rangle \ , \tag{1}$$

where $\overleftrightarrow{\Sigma}$ plays the role of an effective perturbation, related to the average transition matrix $\langle \overleftrightarrow{T} \rangle$ by

$$\overleftrightarrow{\Sigma} = (\overleftrightarrow{1} + \langle \overleftrightarrow{T} \rangle \overleftrightarrow{G}_0)^{-1} \langle \overleftrightarrow{T} \rangle \ . \tag{2}$$

In a multiple-scattering approach:

$$\langle \overleftrightarrow{T} \rangle = \sum_i \langle \overleftrightarrow{T}_i \rangle \tag{3}$$

and

$$\begin{aligned} \langle \overleftrightarrow{T}_i \rangle &= \left\langle (\overleftrightarrow{1} + \sum_{i' \neq i} \overleftrightarrow{T}_{i'} \overleftrightarrow{G}_0) \overleftrightarrow{t}_i \right\rangle \\ &= (\overleftrightarrow{1} + \sum_{i' \neq i} \langle \overleftrightarrow{T}_{i'} \rangle \overleftrightarrow{G}_0) \langle \overleftrightarrow{t}_i \rangle \\ &\quad + \left\langle \sum_{i' \neq i} (\overleftrightarrow{T}_{i'} - \langle \overleftrightarrow{T}_{i'} \rangle)(\overleftrightarrow{t}_i - \langle \overleftrightarrow{t}_i \rangle) \right\rangle \ , \end{aligned} \tag{4}$$

where

$$\overleftrightarrow{t}_i = \overleftrightarrow{V}_i (\overleftrightarrow{1} - \overleftrightarrow{G}_0 \overleftrightarrow{V}_i)^{-1} \tag{5}$$

describes the single-site scattering at the ith defect of the phonon wave scattered by the other defects. Accordingly to MD, the perturbation matrix $\overleftrightarrow{V}$ is

$$\overleftrightarrow{V} = (\overleftrightarrow{M}_0 - \overleftrightarrow{M})\omega^2 = [M_0(\kappa) - M(\kappa)]\omega^2 \delta_{ll'} \delta_{\kappa\kappa'} \delta_{\alpha\alpha'} \ , \tag{6}$$

where M, M_0 are the atomic masses, α, α' are Cartesian indexes, and l, l' and κ, κ' label the unit cells and the sublattices, respectively.

The first term in Eq. (4) describes the scattering of an average incident wave by an atom with an average t matrix. The second term takes into account the correlation between fluctuations in the incident wave and in the atomic t matrix. The single-site approximation (SSA) consists in completely neglecting the correlation term. Under this assumption $\overleftrightarrow{\Sigma}$ takes the final form

$$\overleftrightarrow{\Sigma} = \sum_i \langle \overleftrightarrow{t}_i \rangle (\overleftrightarrow{1} + \overleftrightarrow{G}_0 \langle \overleftrightarrow{t}_i \rangle)^{-1} \ . \tag{7}$$

We point out that these relations hold even if $\overleftrightarrow{G}_0$ represents the Green function of an arbitrary reference crystal. The standard choice for ATA is to take the latter as a periodic crystal with cation masses equal to the weighted average between Ga and Al (VCA). In this case $\overleftrightarrow{\Sigma}$ is exact at both limits of the composition range, if a first-order expansion in the defect concentration is carried out. Therefore, ATA represents a useful interpolation scheme, which is expected, however, to give some problems at $x \cong 0.5$. In particular, it may originate undamped plane-wave excitations outside the frequency spectrum of the reference crystal.[3] This feature would be in contrast with the fact that such plane-wave excitations cannot occur in disordered systems. Actually these shortcomings could be avoided by a self-consistent approach to the SSA, i.e., by making use of the CPA scheme: In this case the reference crystal is chosen in such a way that $\overleftrightarrow{\Sigma} = \overleftrightarrow{0}$.[3] However this approach requires the self-consistent solution of an equation in $\overleftrightarrow{G}_0$ and $\overleftrightarrow{\Sigma}$ which is, in the case of BCM, very cumbersome to handle analytically and prohibitively expensive to solve by numerical iteration in the case of extended-cell systems, like the superlattices studied in paper II. For these reasons we adopt the ATA, whose validity for $Al_xGa_{1-x}As$ is here investigated by comparison to supercell calculations.

Turning to the problem of configurational averages, we take advantage of the translational invariance of $\langle \overleftrightarrow{G} \rangle$ and $\overleftrightarrow{\Sigma}$, and write explicitly

$$\begin{aligned} \langle G_{jj'}(\mathbf{q}\omega) \rangle &= \delta_{jj'} [\omega^2 - \omega_{0j}^2(\mathbf{q}) + i2\omega 0^+]^{-1} \\ &\quad + \sum_{j''} [\omega^2 - \omega_{0j}^2(\mathbf{q}) + i2\omega 0^+]^{-1} \Sigma_{jj''} \\ &\quad \times \langle G_{j''j'}(\mathbf{q}\omega) \rangle \ , \end{aligned} \tag{8}$$

where $\mathbf{q}$ is the wave vector and j the branch index. Finally, the phonon density of states for biatomic mixed crystals is defined as

$$\rho(\omega) = -\frac{\omega}{3\pi N} \mathrm{Im\,Tr} \langle \overleftrightarrow{M} \overleftrightarrow{G} \rangle \tag{9}$$

and the $\langle \overleftrightarrow{M} \overleftrightarrow{G} \rangle$ configuration average can be calculated by means of conditional configuration averaged Green functions expressed in terms of $\langle \overleftrightarrow{G} \rangle$ and $\overleftrightarrow{\Sigma}$ (for an extensive treatment of this subject, see Elliot, Krumhansl, and Leath, Ref. 3).

V. SUPERCELL CALCULATION SCHEME

Our supercell approach consists in a direct diagonalization of a large dynamical matrix, where the mass matrix contains all the information about compositional disorder in the crystal. This technique has been outlined in a previous paper by two of us[22] and here we report only the main ideas.

The first step in this procedure is to construct a force-constant matrix (FCM) $\Phi_{\alpha\beta}(\mathbf{Q}|(\mathbf{J}\kappa)(\mathbf{J}'\kappa'))$ using GaAs parameters only and referring to a unit cell containing a large number of atoms [labeled by the $(\mathbf{J}\kappa)$ index]. This can be done by iterating the calculation of the FCM for the standard GaAs unit cell $\phi_{\alpha\beta}(\mathbf{q}|\kappa\kappa')$ at selected $\mathbf{q}$ points of the original Brillouin zone (OBZ):

$$\Phi_{\alpha\beta}[\mathbf{Q}|(\mathbf{J}\kappa)(\mathbf{J}'\kappa')]=\sum_{q}^{\mathrm{OBZ}}\phi_{\alpha\beta}(\mathbf{q}|\kappa\kappa')e^{i(\mathbf{Q}-\mathbf{q})\cdot[(J_1'-J_1)\mathbf{a}_1+(J_2'-J_2)\mathbf{a}_2+(J_3'-J_3)\mathbf{a}_3+\mathbf{x}(\kappa')-\mathbf{x}(\kappa)]}$$
$$\times\frac{1}{M_1M_2M_3}\left[\sum_{L_1,L_2,L_3}\frac{M_1M_2M_3}{N_1N_2N_3}e^{i(\mathbf{Q}-\mathbf{q})\cdot[L_1M_1\mathbf{a}_1+L_2M_2\mathbf{a}_2+L_3M_3\mathbf{a}_3]}\right]$$
$$=\frac{1}{M_1M_2M_3}\sum_{\mathbf{G}}^{(\mathbf{Q}-\mathbf{G})\in\mathrm{OBZ}}\phi_{\alpha\beta}(\mathbf{Q}-\mathbf{G}|\kappa\kappa')e^{i\mathbf{G}\cdot[(J_1'-J_1)\mathbf{a}_1+(J_2'-J_2)\mathbf{a}_2+(J_3'-J_3)\mathbf{a}_3+\mathbf{x}(\kappa')-\mathbf{x}(\kappa)]}, \tag{10}$$

where $\{\mathbf{a}_1,\mathbf{a}_2,\mathbf{a}_3\}$ are the unit vectors of the (small) original unit cell; $\{M_1\mathbf{a}_1,M_2\mathbf{a}_2,M_3\mathbf{a}_3\}$ are the ones of the extended cell and $\mathbf{G}=m_1\mathbf{B}_1+m_2\mathbf{B}_2+m_3\mathbf{B}_3=(m_1/M_1)\mathbf{b}_1+(m_2/M_2)\mathbf{b}_2+(m_3/M_3)\mathbf{b}_3$ is the generic reciprocal vector of its reduced Brillouin zone. The FCM $\overleftrightarrow{\Phi}$ can be now multiplied by the mass matrix M as

$$M^{-1/2}(J\kappa)\overleftrightarrow{\Phi}M^{-1/2}(J'\kappa'), \tag{11}$$

where a random substitution of Ga masses by Al ones can be performed for a suitable set of lattice sites (J,κ is the cation). The set is selected by a generation of random numbers, which assigns at each (J,κ is the cation) site a real value between 0 and 1. If this latter exceeds x (Al concentration) a Ga mass is assigned, otherwise an Al mass is chosen. This corresponds to a MD approach for the $Al_xG_{1-x}Al$ dynamics. Obviously, the calculation of the optical properties and phonon densities of states requires the evaluation of an average over several different configurations, selected by different runs of the random number generator at fixed x. Here we have considered up to six configurations for each concentration and the minor structures that still remain in our spectra could be washed out by increasing the number of such configurations, if they do not represent some persistent cluster in the alloy.

For the present calculation of the phonon density of states (where only the eigenvalues of the dynamical matrix are required), we extended the three unit vectors of the original unit cell by 6, 8, and 10 times, obtaining a supercell of 960 atoms. However, for the evaluation of the optical properties, the eigenvectors are needed as well, so we reduced the size of the macrocell to 480 atoms for the sake of computer memory limits. This size turns out to be sufficiently large in order to avoid fictitious correlations between neighboring supercells (i.e., the three-dimensional superperiodicity does not affect the results). Moreover, the asymmetric shape of the supercell prevents the sampling of the OBZ from containing equivalent points (i.e., degenerate frequencies) and optimizes the statistic distribution of the normal modes in the SC spectra. The technique outlined here is really convenient in numerical applications only if the cation substitution does not affect the force-constant matrix or, in other words, if the MD approximation does reproduce the experimental features of AlAs. As previously discussed, this is the case of $Al_xGa_{1-x}Al$ and very few other III-V compounds.[12]

VI. DIELECTRIC PROPERTIES

The dielectric function in the spectral region of the lattice vibrations can be expressed as

$$\overleftrightarrow{\epsilon}=\epsilon_\infty\overleftrightarrow{1}+4\pi\overleftrightarrow{\chi}, \tag{12}$$

where ϵ_∞ is the static dielectric constant of the electronic system only and $\overleftrightarrow{\chi}$ is the ionic part of the dielectric susceptibility. The absorption coefficient along the z axis is proportional to $\mathrm{Im}\chi_{\alpha\alpha}(\omega,q_z\to0)(\alpha\alpha=xx,yy)$ and the excitation spectrum for transverse modes is therefore obtained. For what concerns the longitudinal phonons, a quantity which can be helpfully compared to the Raman spectra (except for the relative intensities of the peaks) is

$$-\mathrm{Im}\frac{1}{\epsilon_{zz}(\omega,q_z\to0)}. \tag{13}$$

Calculations for the Raman scattering with the bond polarizability model and the same ATA/SC approach are in progress and will be published elsewhere. The reflectivity can be readily obtained by

$$r=\frac{(1-n_1)^2+n_2^2}{(1+n_1)^2+n_2^2}, \tag{14}$$

where n_1 and n_2 are the real and imaginary parts of the refraction index n, respectively, and $n=\sqrt{\epsilon}$. All the different optical response functions can be easily derived by evaluating the ionic part of the dielectric susceptibility (12) in terms of the effective charges and the Green function:

$$\chi_{\alpha\alpha'}(\omega)=\frac{1}{V}\sum_{l\kappa,l'\kappa',\beta\beta'}Z_{\alpha\beta}(l\kappa)Z_{\alpha'\beta'}(l'\kappa')\times G_{\beta\beta'}(l\kappa,l'\kappa'|\omega). \tag{15}$$

Actually, $\overleftrightarrow{\chi}$ contains the electronic contribution due to the deformation of the electronic wave function produced by the ionic displacements, but does not contain the polarization of the electronic system under the external field with ions at rest. For this reason ϵ_∞ is added separately in Eq. (12). Moreover, we note that $\overleftrightarrow{\chi}$ in Eq. (15) is the response function to the *external* field, while $\overleftrightarrow{\chi}$ in Eq. (12) is the response to the *total* (external plus induced) field. The two quantities coincide for the transverse part of the tensor (zero-induced field). On the other hand, for the longitudinal response the induced field *is not* zero and it is given by the macroscopic field associated to optical

phonons. Consequently, in order to reproduce the correct longitudinal susceptibility in Eq. (12), we have to remove this macroscopic field from the Green function appearing in Eq. (15).

For pure AlAs and GaAs Z is independent of the cell index l and can be estimated by the usual expression[3]

$$\omega_{\mathrm{LO}}^2-\omega_{\mathrm{TO}}^2=\frac{4\pi Z^2}{v_a\mu\epsilon_\infty}\ , \tag{16}$$

which is derived from the Lyddane-Sachs-Teller relation (v_A,μ are the volume and the reduced mass of the unit cell, respectively). Here, by using the experimental values $\epsilon_\infty^{\mathrm{AlAs}}=8.16$ and $\epsilon_\infty^{\mathrm{GaAs}}=10.88$,[23] we obtain $Z_{\mathrm{Al}}=1.875$ and $Z_{\mathrm{Ga}}=2.165$, in units of one electronic charge.

In the mixed crystal we have to consider the configurational average of the dielectric susceptibility, given by

$$\vec{\vec{\chi}}=-\frac{1}{V}\sum_{l\kappa,l'\kappa'}\langle Z(l\kappa)Z(l'\kappa')\vec{\vec{G}}(l\kappa,l'\kappa'|\omega)\rangle\ . \tag{17}$$

We assume that in the mixed crystal $Z(l1)$ is equal to $Z_{\mathrm{Al}}(Z_{\mathrm{Ga}})$ if an Al(Ga) atom is present in the lth cell, while

$$Z(l2)\equiv Z_2=xZ_{\mathrm{Al}}+(1-x)Z_{\mathrm{Ga}} \tag{18}$$

for any cell index l. This assumption introduces the disorder in the effective charges of the metal ions and preserves the neutrality condition taking the VCA effective charge for As. This is actually an approximation, because even the As charge is site dependent in a real system and a straight forward physical consequence of this position is that the intensity of the AlAs-like response turns out to be slightly underestimated, whereas the one of the GaAs-like peaks slightly overestimated. Obviously, the same VCA approach is used also in the definition of the static electronic part of the dielectric constant:

$$\epsilon_\infty=x\epsilon_\infty^{\mathrm{AlAs}}+(1-x)\epsilon_\infty^{\mathrm{GaAs}}\ . \tag{19}$$

For the evaluation of the average $\langle Z\vec{\vec{G}}Z\rangle$ we need to calculate the configurational conditional averages (see Elliot, Krumhansl, and Leath, Ref. 3) of the Green function $\vec{\vec{G}}_d(l1,l'\kappa')$ and $\vec{\vec{G}}_h(l1,l'\kappa')$ where only those configurations with a defect (d) or a host atom (h) at the ($l1$) lattice site are included. We need also the calculation of configuration averages which are conditional on both the first and the second site in each unit cell: They will be denoted by $\vec{\vec{G}}_{ij}$, where i and j take the values h and d for host and defect atom on sublattice $\kappa=1$.

The final expression for $\vec{\vec{\chi}}$ is obtained by Fourier transforming the averaged Green function:

$$\vec{\vec{\chi}}=-\frac{1}{v_A}\left[Z_2^2\langle\vec{\vec{G}}(22|\mathbf{q}\to\mathbf{0})\rangle+\sum_{i=h,d}Z_2Z_i[\langle\vec{\vec{G}}_i(21|\mathbf{q}\to\mathbf{0})\rangle+\langle\vec{\vec{G}}_i(12|\mathbf{q}\to\mathbf{0})\rangle]+\sum_{i,j=h,d}Z_iZ_j\langle\vec{\vec{G}}_{ij}(11|\mathbf{q}\to\mathbf{0})\rangle\right]\ , \tag{20}$$

where $\langle\vec{\vec{G}}_{ij}\rangle$ and $\langle\vec{\vec{G}}_i\rangle$ can be expressed in terms of $\langle\vec{\vec{G}}(\kappa\kappa'|\mathbf{q}\to\mathbf{0})\rangle$ and $\vec{\vec{\Sigma}}(\kappa\kappa'|\mathbf{q}\to\mathbf{0})$, as described by Elliot, Krumhansl, and Leath.[3]

Finally, we remark that the disorder in the effective charges produces a strong enhancement of DATA and DALA structures (up to 300%). Nevertheless, in the $Al_xGa_{1-x}As$ alloy the intensity of DALA and DATA peaks is 100 times weaker than the one of optical peaks: This is a consequence of the small difference in the effective charge of our GaAs and AlAs. In the Raman spectra, on the contrary, the larger inequivalence between GaAs and AlAs polarizabilities makes easily observable DATA, DALA, and even DAO features.[9] Moreover, we note that there is no inconsistency between the choice of the MD approximation and the introduction of the disorder in the effective charges. As a matter of fact, the effective charge enters in the dynamical matrix only through the term Z^2/ϵ_∞. Different Z's are consistent with the same force-constant matrix (supposed unchanged in the MDA) provided that the ϵ_∞ is consistently rescaled, as is the case for AlAs and GaAs compounds.

VII. RESULTS AND DISCUSSION

In this section we report a comparison between ATA and SC calculations for the density of states, $\mathrm{Im}\chi_{xx}(\omega)$, $-\mathrm{Im}[1/\epsilon_{zz}(\omega)]$, and the reflectivity at normal incidence. The calculation of the reference Green function has been performed by a root sampling procedure, involving 64 000 points in the Brillouin zone and a small imaginary part (0.04 THz) has been added to the frequency in order to smooth out the numerical fluctuations, generated by the sampling procedure. The values of Al concentrations tested by ATA ($x=0.0,0.08,0.21,0.38,0.54,0.82,1.0$) are the same of Ilegems and Pearson[8] in order to make a comparison with the experimental reflectivity spectra. The SC results are presented only for three concentrations around 50%: In this range the failure of the ATA should be most evident, whereas this interpolation scheme is fully reliable near the concentration limits $x\to0.0$ and $x\to1.0$.

Figure 1(a) displays the ATA density of states (DOS): By comparing with the SC results [Fig. 1(b)], we note that the acoustic part of the spectrum is very well reproduced up to 6 THz. In particular, we distinguish TA contribution from L, X, and K points of the bulk Brillouin zone in the broad structure near 3 THz and a sharper LA peak just below 6 THz. A slight stiffening of both, by increasing the AlAs concentration, is also well reproduced. In the optical region, however, the GaAs-like peak displays a reversed-intensity trend from $x=0.38$ to 0.82 and the gap between GaAs-like and AlAs-like optical modes turns out to be smaller than the SC one. These effects are originated by the fact that the multiple-scattering pertur-

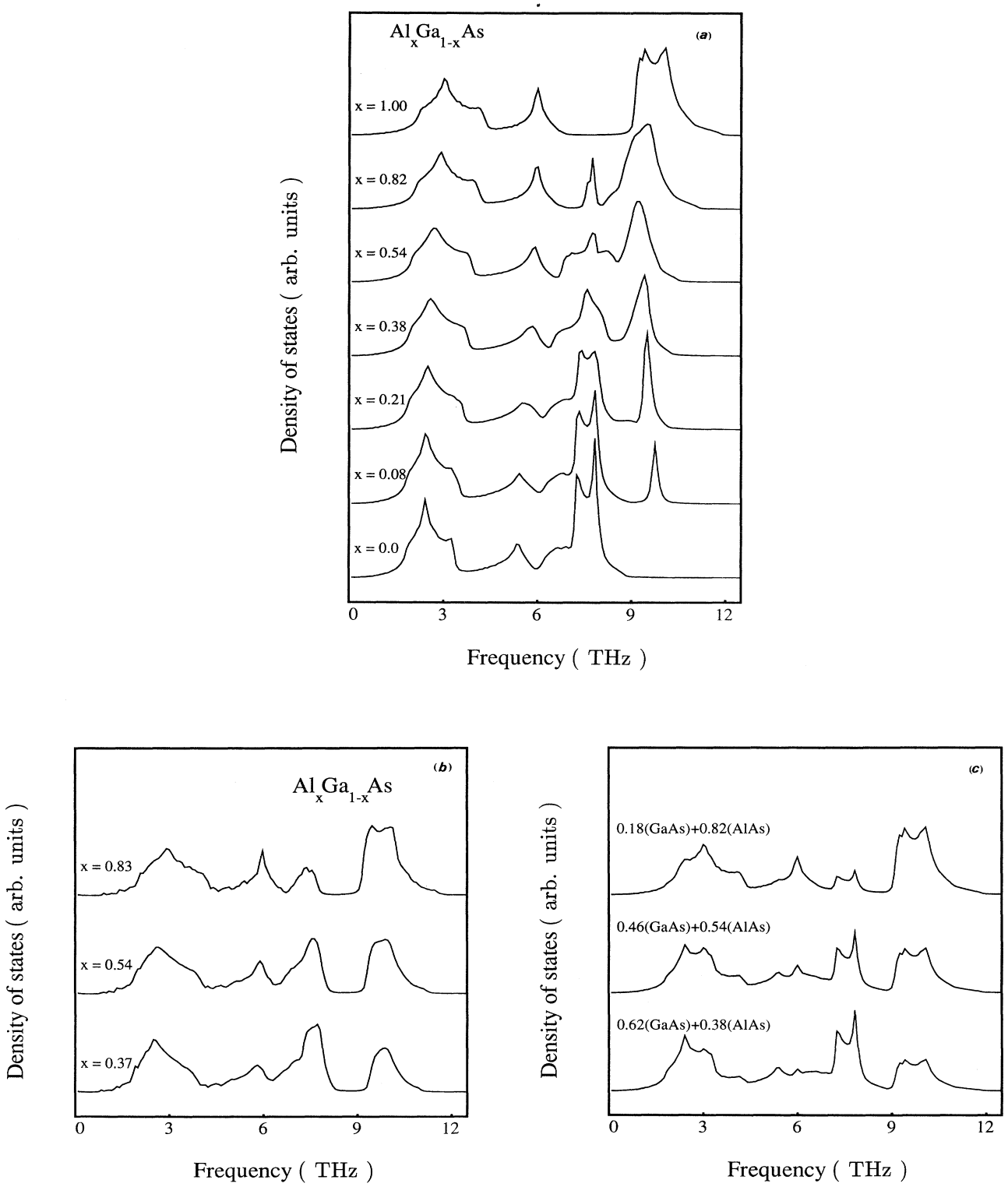

FIG. 1. (a) Phonon density of states for the $Al_xGa_{1-x}As$ homogeneous alloy, calculated by the ATA. The different Al concentrations correspond to the measured ones by Ilegems and Pearson (Ref. 7). (b) Phonon density of states for the $Al_xGa_{1-x}As$ homogeneous alloy, calculated by a supercell of 960 atoms, in the 50% concentration range. For each concentration the average has been evaluated over four different configurations. (c) Superposition of bulk AlAs and GaAs density of states. Different weighting factors for the two bulks have been used: GaAs=0.18 and AlAs=0.82 (top); GaAs=0.46 and AlAs=0.54 (center); GaAs=0.62 and AlAs=0.38 (bottom).

bation provided by the ATA in the region of maximum disorder, hardly manages to provide a two-mode behavior out of the VCA unperturbed crystal, where no gap is present between GaAs-like and AlAs-like modes (this is particularly true for the GaAs-like resonance). A useful comparison can be made with the normalized superposition of pure GaAs and pure AlAs BCM phonon densities [Fig. 1(c)]. In such a very crude approximation (the *persistent features* scheme of Ref. 10) we note that the optical gap (two-mode behavior) is quite well reproduced, although a doubling of the main structures is present and the acoustic part is only poorly reproduced. Generally speaking, the superposition of the bulk DOS's is very similar to the SC calculations in the optical region. Still we note the effects of the alloy configuration in the presence of (i) a low-frequency shoulder in the GaAs-like peak; (ii) the filling of the dip in the AlAs-like structure. The same alloy modes have been found by Kobayashi, Dow, and O'Reilly[10] by a recursion-method technique that allows for a detailed attribution of spectral features to vibrations of specific cluster environments. According to Ref. 10 we identify the following alloy modes: (i) the low-frequency shoulder of GaAs peaks [see Fig. 1(b)] as due to vibrations of Ga atoms surrounded by Al atoms as second nearest neighbors and vibrations of central As atoms with Al atoms as first nearest neighbors; (ii) the filling of the dip in the AlAs-like peak as due to vibrations of Al atoms with Ga atoms as second nearest neighbors.

The DOS collects contributions from the whole Brillouin zone, so that the dispersion (and linewidth) of the modes affects quite heavily the resulting spectra. Therefore we expect that the susceptibility and the dielectric function at zone center ($\mathbf{q}=0$) should display minor differences in the optical region between ATA and SC results. This is actually seen in Fig. 2, where a comparison of the ATA versus SC for the $\mathrm{Im}\vec{\chi}$ function is displayed. Choosing SC spectra as a benchmark calculation [Fig. 2(b)], we see that the ATA results [Fig. 2(a)] give a good description of the DATA and DALA structures at low frequency (here magnified 100 times). Their line shape is rather similar to the acoustic part of the phonon density of states[9] [see Figs. 1(a) and 1(b)]: Disorder in the effective charges (here included) strongly contribute to enhance the intensity of the $\mathbf{q}\neq 0$ peaks (up to 300%). Even the interchange in intensity of the two peaks around 3 THz [TA(X) and TA(K)] is well reproduced when the Al concentration ranges in the interval $0.38 < x < 0.82$. In the optical side the frequency position of the peaks is now in good agreement even if the intensity and the linewidth of the GaAs-like peak is still poorly described by ATA. In particular, we note that the GaAs-like peaks of Fig. 2(b) (SC) do display a low-frequency shoulder by activation of $\mathbf{q}\neq 0$ TO modes for maximum disorder concentration ($x=0.52$). These features are masked in the ATA approach by the spurious broadening originated by VCA. As already mentioned, the configurational averages performed in the SC calculation are not able to entirely eliminate the statistical fluctuations, still present all throughout the spectra: These minor kinks, however, may contain some intrinsic feature, as we will see in the

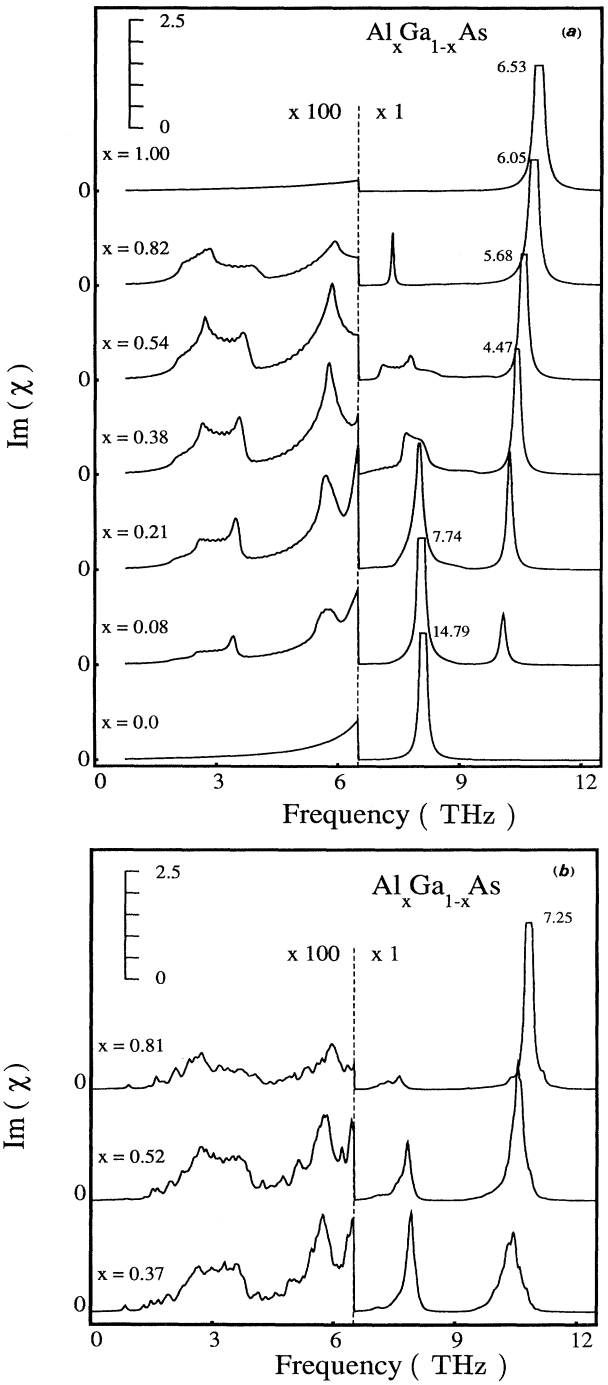

FIG. 2. (a) Function $\mathrm{Im}\chi_{xx}(\omega)$ calculated by ATA for the same Al concentrations of Fig. 1(a). The spectrum has been magnified by a factor of 100 for frequencies less than 6.3 THz. The absolute intensity of the truncated optical peaks has been explicitly indicated. We report, also, the scale for the vertical axis in the top left corner of the picture. (b) Function $\mathrm{Im}\chi_{xx}(\omega)$ calculated by a supercell of 480 atoms, in the 50% concentration range. For each concentration the average has been evaluated over six different configurations. The spectrum has been magnified by a factor of 100 for frequencies less than 6.3 THz. The absolute intensity of the truncated optical peaks has been explicitly indicated.

longitudinal case.

Figure 3 reports the longitudinal-vibration spectra at zone center: We plot the function $-\mathrm{Im}(1/\epsilon_{zz})$ which is qualitatively comparable to the Raman spectra in backscattering geometry.[6,9] We note that the same comments that we made for $\mathrm{Im}\chi_{xx}(\omega)$ still hold in this case: The

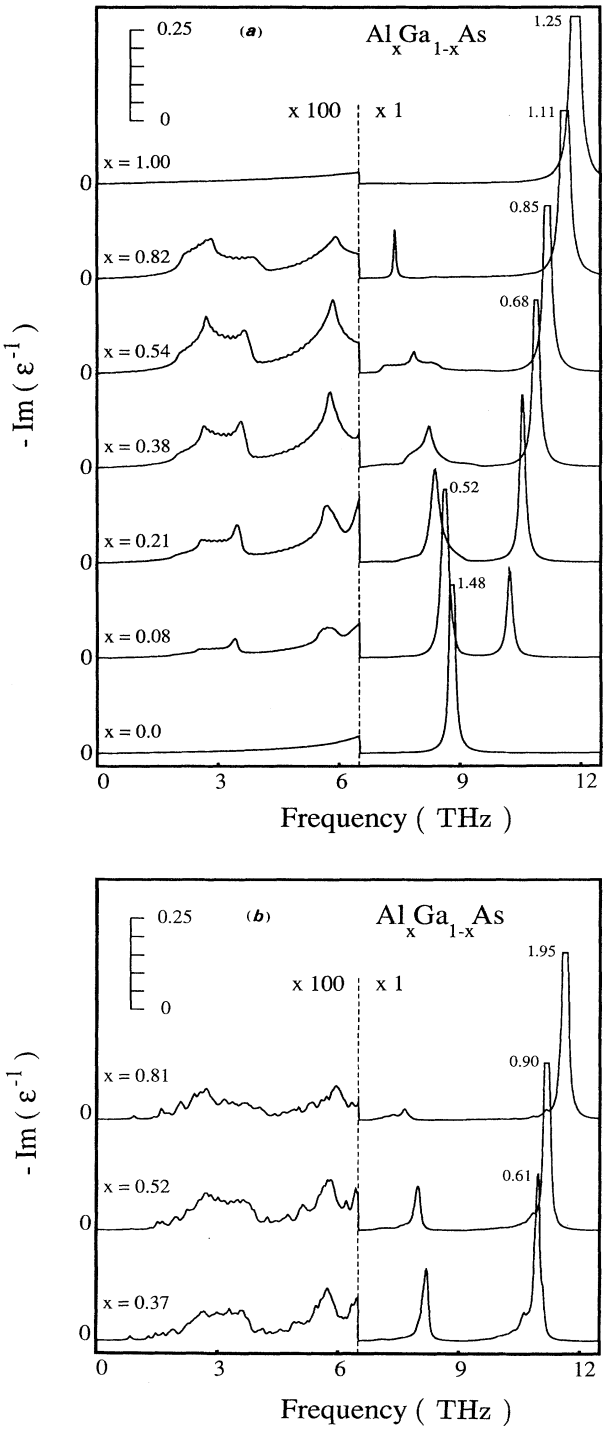

FIG. 3. (a) The same as Fig. 2(a) for the function $-\mathrm{Im}(1/\epsilon_{zz})$. (b) The same as Fig. 2(b) for the function $-\mathrm{Im}(1/\epsilon_{zz})$.

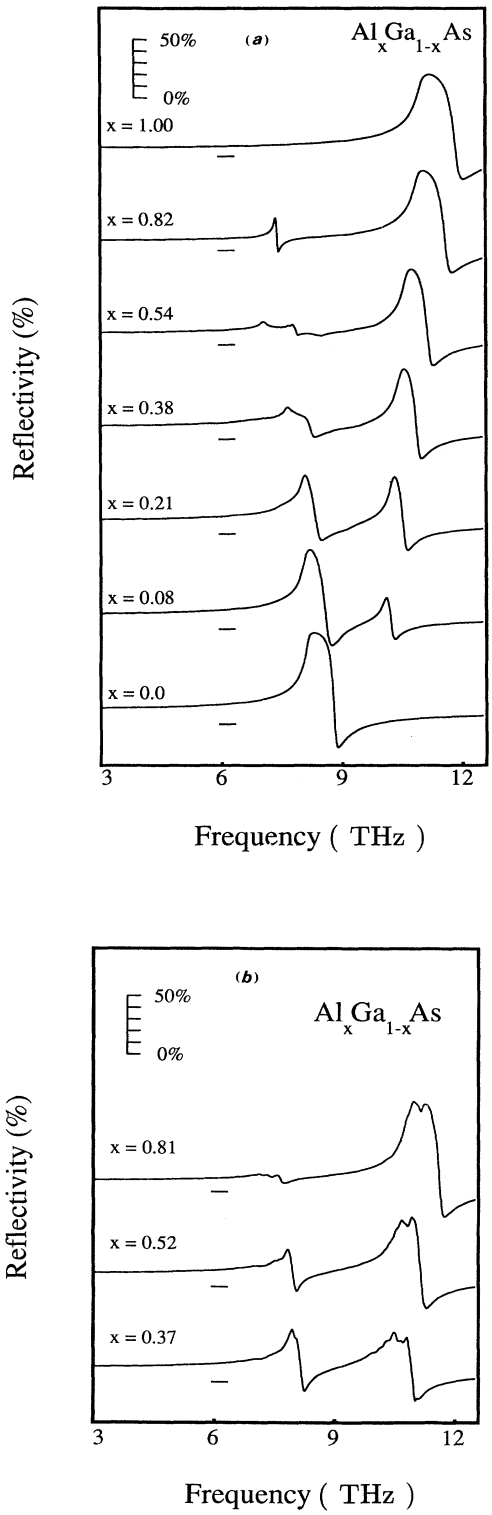

FIG. 4. (a) Reflectivity spectrum for the $Al_xGa_{1-x}As$ homogeneous alloy calculated by the ATA for the same Al concentrations of Fig. 1(a). The horizontal bars indicate the 20% reflectivity level. (b) Reflectivity spectrum for the $Al_xGa_{1-x}As$ homogeneous alloy calculated by a supercell of 480 atoms, in the 50% concentration range. For each concentration the average has been evaluated over six different configurations.

AlAs-like peak, in particular, does display the correct shift in frequency with concentration and both ATA and SC results do agree with experimental results within a few percent.

In our calculation of $-\mathrm{Im}(1/\epsilon_{zz})$ the appearance of disorder-activated TO modes is not so evident as in the Raman measurements[6,9]: They are barely visible in the SC case and an expansion by 100 times would be necessary, as in the DALA and DATA case. However, an interesting persistent feature is seen in Fig. 3(b), just below the LO AlAs peak. This peak is present for all the configurations on which we have made the average and since it is more evident for smaller Al concentration (and not present in the ATA calculation), we interpret it as due to the cluster of Ga second neighbors around an Al impurity, according to Kobayashi, Dow, and O'Reilly.[10] Moreover its frequency position is somehow midway between the TO band and the LO AlAs peak. Calculation of Raman intensities will hardly attribute the origin of such a feature.

One more comment should be added with regard to the fairly good description of the trend in the frequency shift of both TO and LO peaks (either in the case of GaAs and AlAs). Our results satisfactorily agree with the experiments[8,9] even in predicting the nearly linear dependence of LO GaAs-like and TO AlAs-like peaks, in contrast to the nonlinear dependence of TO GaAs-like and LO AlAs-like ones. They indicate that the dynamical model and the ATA scheme correctly take into account the correlations among defects. In fact, the physical origin of the shift (toward higher frequencies) of the optical peaks, when the concentration of defects increases, relies in the strengthening of the dynamical correlation among different defect sites. As expected, the LO-TO splitting increases from the low-concentration limit to the pure compound. This can be easily understood noting that the larger the number of correlated defects, the larger is the macroscopic electric field. The discrepancies between theoretical and experimental positions of the peaks are always smaller than 5%, with a systematical theoretical underestimation. This misfit is mainly due to the dynamics. As a matter of fact, an error of about 5% is present also in the evaluation of the single-impurity localized modes: The calculated defect mode of Al in $Al_{0.01}Ga_{0.99}As$ and of Ga in $Al_{0.99}Ga_{0.01}As$ are, respectively, 7.3 and 10.0 THz against the experimental values of 7.7 and 10.7 THz.[8,9] Since in the single-impurity limit the ATA approximation is exact, the discrepancy has to be attributed to a failure of the isotopic approximation (MD) and the BCM.

In Fig. 4 we display the reflectivity of the $Al_xGa_{1-x}As$ system: Here both longitudinal and transverse modes contribute to the total spectrum through the real and imaginary part of the refractive index [see Eq. (14)]. The ATA results [Fig. 4(a)] well agree with the experimental data of Ref. 8 even if the intensity of the GaAs-like peak is somehow underestimated with respect to the AlAs-like one. This is not due to the approximation for the effective charges. We proved that by calculating the reflectivity spectra with the charge of metallic ions set equal to Z_{Ga} for all lattice sites: The results show that the GaAs-like peak is only poorly affected, remaining underestimated by a factor of about 10%. The same result holds for the AlAs-like structure [in this case we put $Z(l1)=Z_{Al}$]. Our conclusion is that the disagreement is implicit in the ATA, which over(under)-estimates the damping produced by the disorder in the GaAs(AlAs) band: In fact, as previously mentioned, within the ATA the localization occurring outside the frequency spectrum of the reference crystal has a plane-wave character. Finally, we remark that at $x=0.54$ concentration a double structure appears in the calculated ATA GaAs-like band, having no counterpart in the experimental spectra. Figure 4(b) clearly shows that all the ATA drawbacks are overcome by the supercell calculation that turns out to be in very good agreement with experiments, especially with the more accurate measurement by Kim and Spitzer.[8]

In conclusion, the ATA approach is demonstrated to be a sufficiently reliable technique for the investigation of the most important features in disordered materials (disorder-activated bands and frequency positions of the reststrahlen peaks). In regards to the intensities in the 50% concentration range and any cluster contribution to the optical activity, it is not adequate. Therefore a suitable strategy for more complicated systems, such as the mixed crystal superlattice which are studied in the following paper (II), will be to use ATA for the interpretation of the main trends occurring by changing composition and superperiodicity, and to perform more time-consuming SC calculations only in particularly interesting configurations.

ACKNOWLEDGMENTS

Work was partially supported by Consiglio Nazionale delle Recerche, in the framework of Progetto Finalizzato Materiali Speciali per Tecnologie Avanzate and Comitato Scienze Fisiche for Cray Y-MP calculations.

*Present address: Dipartimento di Fisica, via Celoria 16, I-20133 Milano, Italy.

[1]M. Bernasconi, L. Colombo, and L. Miglio, following paper, Phys. Rev. B **43**, 14 457 (1991).

[2]A. S. Barker and A. J. Sievers, Rev. Mod. Phys. **47**, Suppl. **2**, S1 (1975).

[3]R. J. Elliott, J. A. Krumhansl, and P. L. Leath, Rev. Mod. Phys. **46**, 465 (1974); J. Bernasconi, in *Phonons: Theory and Experiment III,* edited by P. Brüesch (Springer, Heidelberg, 1987), p 140; H. Böttger, *Principles of the Theory of Lattice Dynamics* (Akademic, Berlin, 1983).

[4]P. N. Sen and W. M. Hartman, Phys. Rev. B **9**, 367 (1974).

[5]R. Bonneville, Phys. Rev. B **29**, 907 (1984); *ibid.* **24**, 1987 (1981).

[6]Pudong Lao, Wade C. Tang, A. Madukar, and P. Chen, J. Appl. Phys. **65**, 1676 (1989).

[7]D. W. Taylor, in *Optical Properties of Mixed Crystals,* edited by R. J. Elliott and I. P. Ipatova (North-Holland, Amsterdam,

1988), p. 35.
[8]M. Ilegems and G. L. Pearson, Phys. Rev. B **1**, 1576 (1970); O. K. Kim and W. G. Spitzer, J. Appl. Phys. **50**, 4362 (1979).
[9]N. Saint-Cricq, G. Landa, J. B. Renucci, I. Hardy, and A. Muñoz-Yagne, J. Appl. Phys. **61**, 1206 (1987); R. Carles, N. Saint-Cricq, A. Zwick, M. A. Renucci, and J. B. Renucci, Il Nuovo Cimento **2D**, 1712 (1982).
[10]A. Kobayashi, J. D. Dow, and E. P. O'Reilly, Superlatt. Microstruct. **1**, 471 (1985).
[11]D. N. Talwar, M. Vandevyver, and M. Zigone, Phys. Rev. B **23**, 1743 (1981).
[12]S. Baroni, P. Giannozzi, and A. Testa, Phys. Rev. Lett. **58**, 1861 (1987); S. Baroni, S. de Gironcoli, and P. Giannozzi, *ibid.* **65**, 84 (1990); P. Pavone, thesis of Magister Philosophiae, Scuola Internazionale Superiore di Studi Avanzati, 1989.
[13]W. Weber, Phys. Rev. B **15**, 4789 (1977).
[14]K. C. Rustagi and W. Weber, Solid State Commun. **18**, 673 (1976).
[15]J. R. Chekikowsky and Marvin L. Cohen, Phys. Rev. B **14**, 556 (1976).
[16]A. A. Maradudin, E. W. Montroll, G. H. Weiss, and I. P. Ipatova, *Theory of Lattice Dynamics in the Harmonic Approximation,* Solid State Physics Vol. **3** (Academic, New York, 1971).
[17]A. Fleszar and R. Resta, Phys. Rev. B **34**, 7140 (1986).
[18]L. Colombo and L. Miglio, Phys. Scr. **40**, 238 (1989).
[19]D. Strauch, B. Dorner, J. Phys. Condens. Matter **2**, 1457 (1990).
[20]H. Biltz, D. Strauch, R. K. Wehner, A. Ontan and R. J. Chicotka, Phys. Rev. B **10**, 591 (1974).
[21]*Encylopedia of Physics,* edited by S. Flügge and L. Genzel, Light and Matter Id, Vol. XXV/2d (Springer-Verlag, Berlin, 1984).
[22]L. Miglio and L. Colombo, Superlatt. Microstruct. **7**, 139 (1990).
[23]*Semiconductors: Intrinsic Properties of Group IV Elements and III-VI, II-VI and I-VII Compounds,* edited by O. Madelung, Landolt-Börnstein, New Series Group III, Vol. 22a (Springer-Verlag, Berlin, 1987).